

Flow Control Over the NACA 4415 Airfoil using Micro Cylinder- A Computational Study

Gokul Anand

Turbulence & Flow control Lab, School of Mechanical Engineering,
SASTRA Deemed University.

Abstract:- The effect of passive flow control methods is widely studied and investigated due to its slight variation in the geometrical parameters with significant improvement in the aerodynamic efficiency. The computational study of the flow over the NACA 4415 airfoil section with the microcylinders placed, upstream of the leading edge at the $Re = 3.3 \times 10^5$ was investigated. The physical model of the problem was solved by Reynold's Averaged Navier Stokes Equation (RANS) and turbulence model was generated with standard $k-\epsilon$ (2 equations) turbulence model. The airfoil section was simulated with and without (baseline model) microcylinder along with two variations of diameter. The result shows that the increase in the diameter of the microcylinder delays the stall phenomenon by reducing the separation region in the range of 15° to 25° .

Keywords : Micro cylinder, passive flow control, stall delay

1. INTRODUCTION:

Several studies and methods are still under development to improve the aerodynamic efficiency of the airfoil, which is primarily used in aircraft wings, wind turbine blades and so on. The formation of a wake region in the suction surface of airfoil when it pitches up to higher angles of attack is the highly unavoidable situation. So the passive way of energizing the flow around the airfoil is necessary which significantly alters the aerodynamic characteristics. One of the ways for vitalizing the flow field so that it may be more attached with the airfoil in the downstream is by utilizing the diverse dimensions of microcylinders and placing them near the leading edge of the airfoil. The need to know how well the enhancement of the aerodynamic characteristics can be achieved by the passive methods lies in the improvements in the efficiency of the aircraft. Some of the computational studies on passive flow control are as follows. Computational analysis of the flow over the NACA 0012 at $Re = 6 \times 10^6$ was done by Dahai Luo and et al [1]. In that analysis, the RANS calculations and Spalart-Allmaras (SA) model were used. Menter's $k-\omega$ shear-stress transport (SST) model was also used for comparison. They found that narrow spacing ($s/c < 0.01$) and very less diameter of the cylinder ($D/c = 0.01$) leads to a considerable decrease in lift coefficient. The stall separation region gets varied with different airfoils, spacing, and diameter of the cylinder. Another computational analysis on NREL S809 wind turbine airfoil at $Re = 1 \times 10^6$ in the range of $\alpha = 10^\circ - 24^\circ$ by Xuyang Shi and et al [2]. They found that the aerodynamic characteristics were improved while using oscillating microcylinder instead of a static microcylinder. Similarly,

the other works related to passive flow such as vortex cylinders, square rods in front of bluff bodies were also done, to reduce the wake region.

2. COMPUTATIONAL METHODOLOGY:

2.1. MODEL DESCRIPTION

The NACA 4415 airfoil was chosen for this computational work. The span of the airfoil in the computational domain is 0.3 m and the ends of the airfoil model are closed by the walls in the computational domain which results in the absence of the wingtip vortices. The chord of the airfoil is 0.1 m. By making the adjustments in the dimensions of the microcylinder, the flow field alters significantly. The two different dimensions of the microcylinder are 0.5 mm and 1 mm. The microcylinder is placed at 5 mm in the negative x-axis and 5 mm in the positive y-axis near the leading edge of the airfoil. This computational study was done at the Reynolds number 3.5×10^5 . The baseline case without microcylinder is simulated and tested for the same Reynolds number for the comparison of the data.

2.2 GRID GENERATION:

In this computational study, the adaptive grid was generated around the microcylinders and the airfoil. In the near boundary of the airfoil and microcylinder, the finer grids are used in order to get the high accuracy flow field data in both streamline and wall-normal. The chord length of the NACA 4415 airfoil is $c = 0.1$ m, the computational domain extends $5c$ from the airfoil leading edge at $1c$. The unstructured mesh is generated around all solid surfaces. The initial grid count normal to the wall is set to be 100. The flow field parameters get varied around the surface of the airfoil compared to the far field conditions which significantly provides the information regarding the flow. Flow around the microcylinder which is nearer to the leading edge and the flow variation in trailing edge greatly influence the computational simulation.

2.3 GOVERNING EQUATION AND TURBULENCE MODEL:

The physical model is considered to have the incompressible flow generated by the wind tunnel. The governing equation for this problem is Reynolds averaged two dimensional viscous incompressible Navier- Stokes equation, whose mathematical form as follows:

Continuity equation:

$$\frac{\partial(u_x)}{\partial x} + \frac{\partial(u_y)}{\partial y} = 0$$

Two-dimensional viscous incompressible Navier–Stokes equation:

$$\frac{\partial(\rho u_x)}{\partial t} + \frac{u_x \partial(\rho u_x)}{\partial x} + \frac{u_y \partial(\rho u_x)}{\partial y} = -\frac{\partial p}{\partial x} + \mu \left(\frac{\partial^2 u_x}{\partial x^2} + \frac{\partial^2 u_x}{\partial y^2} \right) \tag{2}$$

$$\frac{\partial(\rho u_y)}{\partial t} + \frac{u_x \partial(\rho u_y)}{\partial x} + \frac{u_y \partial(\rho u_y)}{\partial y} = -\frac{\partial p}{\partial y} + \mu \left(\frac{\partial^2 u_y}{\partial x^2} + \frac{\partial^2 u_y}{\partial y^2} \right) \tag{3}$$

For the simulation of the airfoil and the microcylinder, the standard k-ε model was used everywhere in the low-velocity flow field. Near-wall is treated with standard wall functions. The transport equation of the k-ε model used is: For turbulent kinetic energy k,

$$\rho \epsilon - Y_M + S_k \tag{4}$$

For dissipation ε,

$$C_{1\epsilon} \frac{\epsilon}{k} (P_k + C_{3\epsilon} P_b) - C_{2\epsilon} \rho \frac{\epsilon^2}{k} + S_\epsilon \tag{5}$$

$C_{1\epsilon} = 1.44, C_{2\epsilon} = 1.92, C_\mu = 0.09, \sigma_k = 1.0, \sigma_\epsilon = 1.3$

2.4 SOLUTION METHODOLOGY

A no-slip adiabatic solid wall condition is adopted for both the airfoil and micro-cylinder surface. The free-stream Mach number is fixed at $M = 0.14693$. The Reynolds number based on the airfoil chord length c is fixed at $Re = 3.3 \times 10^5$. The coordinate system origin is set at the starting vertex point of control volume and the coordinate of the micro-cylinder center is denoted by (X, Y) . k-ε (two-equation) turbulence model was adopted and based on Pressure-based, SIMPLE algorithm was adopted. Air was considered as material. Momentum equations, turbulent kinetic energy equations, and dissipation terms all adopt the first-order upwind style. Discretization method used for pressure momentum turbulent kinetic and dissipation rate is first order upwind. AMG method of stabilization is used and smoother type is Gauss-Seidel. A Reference frame is set relative to the cell zone.

RESULTS AND DISCUSSION :

CHANGES IN THE AERODYNAMIC CHARACTERISTICS USING THE MICROCYLINDER:

(1)

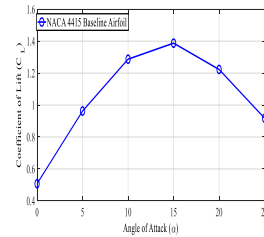


FIG. 1.1 NACA 4415 BASELINE AIRFOIL COEFFICIENT OF LIFT (C_L) VS ANGLE OF ATTACK (α)

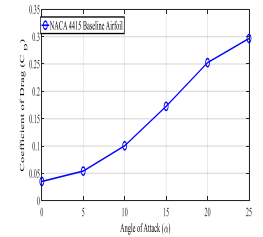


FIG. 2.1 NACA 4415 BASELINE AIRFOIL COEFFICIENT OF DRAG (C_D) VS ANGLE OF ATTACK (α)

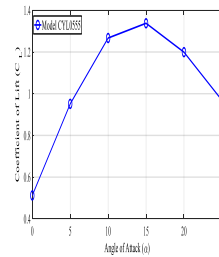


FIG. 1.2. NACA 4415 AIRFOIL WITH 1MM DIAMETER COEFFICIENT OF LIFT(C_L) VS ANGLE OF ATTACK(α)

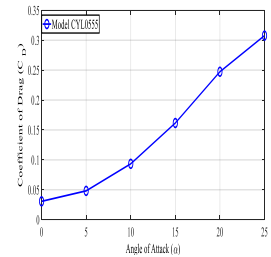


FIG. 2.2. NACA 4415 AIRFOIL WITH 1MM DIAMETER COEFFICIENT OF DRAG(C_D) VS ANGLE OF ATTACK(α)

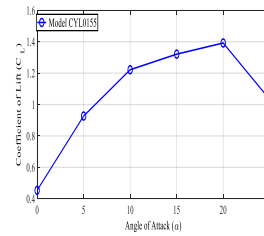


FIG. 1.3. NACA 4415 AIRFOIL WITH 2MM DIAMETER COEFFICIENT OF LIFT(C_L) VS ANGLE OF ATTACK(α)

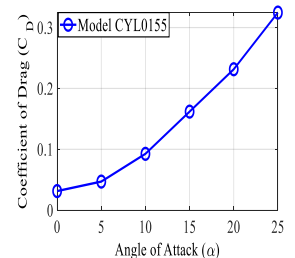


FIG. 2.2. NACA 4415 AIRFOIL WITH 2MM DIAMETER COEFFICIENT OF DRAG (C_D) VS ANGLE OF ATTACK(α)

Figure 1.1 to 1.3 describes the Coefficient of lift distribution for a range of the angles of attack starting from 0° to 25°. The C_L distribution of the baseline airfoil shows that the stall occurs at α= 15° with the maximum C_L value 1.39. In the presence of microcylinder ahead of the leading edge at optimum position and size significantly delays the stall phenomenon. This statement is substantiated by the above figure 1.3, the microcylinder with 2 mm indicates the maximum value of C_L=1.4 at α=20° which was the stall angle for this case. Therefore the increase in the size of microcylinder greatly energized the flow field on the upper surface of the airfoil which resulted in the more attachment of the flow throughout the downstream of the airfoil by

delaying the flow separation. On the other hand, the drag slightly increases compared to the baseline case, due to the presence of the microcylinder in the upstream of the leading edge of the airfoil. This can be found from the above-mentioned figures 2.1 to 2.3. The drag of the baseline case, from the fig 2.1 ranges from 0.04 to 0.29. But from the figures 2.2 and 2.3 the drag range were 0.04 to 0.31 and 0.04 to 0.325. This clearly indicates that the drag increases when the microcylinder is placed in upstream of the leading edge of the airfoil. But at the angle of attack 20° , the drag for the baseline case, 1mm and 2 mm diameter cases were 0.24, 0.245 and 0.22 respectively. This may be the optimum angle of attack of the airfoil with the 2mm diameter microcylinder produces the high lift and less drag.

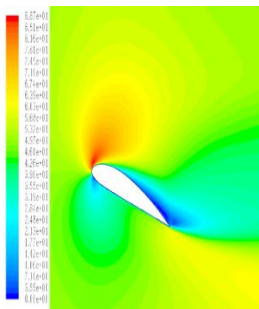


FIG3.1 VELOCITY CONTOUR OF AIRFOIL WITHOUT MICROCYLINDER AT $\alpha=20^\circ$

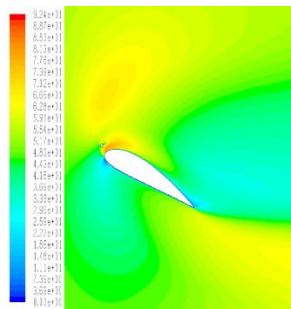


FIG3.2 VELOCITY CONTOUR OF AIRFOIL WITH MICRO CYLINDER OF 2MM DIAMETER AT $\alpha=20^\circ$

This statement is substantiated by the above figure 1.3, the microcylinder with 2 mm indicates the maximum value of $C_L=1.4$ at $\alpha=20^\circ$ which was the stall angle for this case. Therefore the increase in the size of microcylinder greatly energized the flow field on the upper surface of the airfoil which resulted in the more attachment of the flow throughout the downstream of the airfoil by delaying the flow separation. On the other hand, the drag slightly increases compared to the baseline case, due to the presence of the microcylinder in the upstream of the leading edge of the airfoil.

From the above figures 3.1 and 3.2, it can be found that at the angle of attack $\alpha=20^\circ$, in the case without microcylinder the flow on the suction surface has low velocity which shows that the flow was separated. But in the case with microcylinder, the velocity of the flow on the suction surface is much higher compared to its baseline model due to the momentum imparted by the microcylinder. Hence, the flow remains attached which can be clearly seen in the fig 3.2.

CONCLUSION:

The following conclusions were made for the NACA 4415 airfoil which was computationally studied in the range 0° - 25° angle of attack at $Re= 3.3 \times 10^5$:

- The increment in the lift coefficient is purely based on the spacing and diameter of the microcylinder near the

leading edge. The positioning of the microcylinder should be on the suction surface near the leading edge. In this report, the microcylinder was in the position of negative x-axis 5 mm and positive y-axis 5 mm. The results showed that the lift coefficient is more for the diameter 2mm microcylinder compared to the diameter 1mm microcylinder and baseline case. From the velocity contours, it can be found that the presence of the microcylinder significantly makes the flow streamlined over the suction surface and delays the stall phenomenon by maximum $\alpha=5^\circ$.

- The drag coefficient was increased at higher angles since the stalling region makes the aerodynamic loads act majorly in the drag direction.
- At the angle of attack 20° , the lift increases which was shown in the figures from 1.1 to 1.3. Similarly, the drag decreases in this angle of attack which was shown in the figures from 2.1 to 2.3. In this report, the optimum angle of attack for this airfoil- microcylinder (2 mm diameter) combination is $\alpha=20^\circ$.

REFERENCES :

- [1] Dahai Luo, Diangui Huang, and Xiaojing Sun, 2017. "Passive flow control of a stalled airfoil using a microcylinder" Journal of Wind Engineering & Industrial Aerodynamics 170: 256–273.
- [2] Xuyang Shi, Shuai Xu, Li Ding, and Diangui Huang, 2019. "Passive flow control of a stalled airfoil using an oscillating micro-cylinder". Computers and Fluids 178:152–165.
- [3] Haipeng Wang, Bo Zhang, Qinggang Qiu and Xiang Xu., "Flow control on the NREL S809 wind turbine airfoil using vortex generators" Energy:1-12
- [4] Christoph Brucker and Christoph Weidner., 2014. "Influence of self-adaptive hairy flaps on the stall delay of an airfoil in ramp-up motion" Journal of Fluids and Structures 47: 31–40.
- [5] Julien Favier, Antoine Dauptain, Davide Basse and Alessandro Bottaro., 2009. "Passive separation control using a self-adaptive hairy coating" Journal of Fluid Mechanics 627: 451–483.